

ORIGINAL ARTICLE

# Generation of a mouse model of primary hyperoxaluria type 1 *via* CRISPR/Cas9 mediated gene editing

Kimberly A. Coughlan<sup>1</sup>, Rajanikanth J. Maganti<sup>1</sup>, Andrea Frassetto<sup>1</sup>, Christine M. DeAntonis<sup>1</sup>, Meredith Wolfrom<sup>1</sup>, Anne-Renee Graham<sup>1</sup>, Shawn M. Hillier<sup>1</sup>, Steven Fortucci<sup>1</sup>, Hoor Al Jandal<sup>1</sup>, Sue-Jean Hong<sup>1</sup>, Paloma H. Giangrande<sup>1</sup>, Paolo G. V. Martini<sup>1\*</sup>

## ABSTRACT

**Background:** Primary Hyperoxaluria Type 1 (PH1) is an inborn error of metabolism caused by mutations in the *AGXT* gene, which encodes for the hepatocyte-specific enzyme alanine: glyoxylate aminotransferase (AGT). AGT catalyzes the conversion of glyoxylate to glycine in the peroxisome and prevents the build-up of oxalate which occurs in PH1. This causes nephrocalcinosis, systemic oxalosis, and end-stage renal disease. Currently, liver transplant is the only available curative treatment. Although a mouse model has previously been generated, the severity of the reported disease phenotype varies, and a better understanding of the genotype-phenotype relationship in both the mouse model and human disease is needed.

**Methodology:** We developed an *Agxt*<sup>-/-</sup> mouse model using CRISPR/Cas9-mediated gene editing. We performed a natural history study and ethylene glycol (EG) challenge to evaluate the phenotype of this mouse.

**Results:** *Agxt*<sup>-/-</sup> mice had elevated plasma glycolate, urine glycolate, and urine oxalate levels compared to *Agxt*<sup>+/+</sup> mice. A small subset of *Agxt*<sup>-/-</sup> mice developed minimal nephrocalcinosis (1/8 at 12 weeks, 1/8 at 26 weeks, 0/8 at 39 weeks, and 3/7 at 52 weeks of age). When challenged with 0.7% or 1.2% EG in drinking water for 3 weeks, 2/10 *Agxt*<sup>-/-</sup> mice developed nephrocalcinosis. *Agxt2* mRNA and protein expression were unchanged between *Agxt*<sup>-/-</sup> and *Agxt*<sup>+/+</sup> mice. Hydroxy acid oxidase 1 (*Hao1*) messenger ribonucleic acid (mRNA) levels were unchanged, but the corresponding glycolate oxidase protein was increased in *Agxt*<sup>-/-</sup> mice.

**Conclusion:** We have created an *Agxt*<sup>-/-</sup> mouse model which resembles much of the clinical phenotype of PH1 patients and will be a useful tool in developing novel therapies for this devastating disease.

**Keywords:** Primary hyperoxaluria type 1, CRISPR/Cas9, nephrocalcinosis, inborn error of metabolism.

## Introduction

Primary hyperoxalurias (PH) are a group of autosomal recessive disorders of glyoxylate metabolism characterized by an overproduction of oxalate, a metabolic end-product normally excreted in the urine. There are three types of PH, the most common and severe of which is Primary Hyperoxaluria Type 1 (PH1) (1–3). PH1 is caused by mutations in the *AGXT* gene, which encodes for the hepatocyte-specific enzyme alanine: glyoxylate aminotransferase (AGT) (4). AGT normally functions to convert alanine and glyoxylate into pyruvate and glycine, which are then used in other metabolic pathways or easily excreted. However, in the absence of functional AGT, glyoxylate is converted to oxalate, which can only be excreted in the urine. Overproduction

of oxalate from hepatocytes leads to precipitation of calcium oxalate (CaOx) in the kidneys and urinary tract, causing kidney and bladder stones and eventually end-stage renal disease, systemic oxalosis, and death (1). The enzyme is localized in peroxisomes of hepatocytes in humans, whereas the mouse *Agxt* gene has dual

**Correspondence to:** Paolo G. V. Martini

\*Rare Diseases, Moderna Inc, Cambridge, MA.

**Email:** Paolo.Martini@modernatx.com

Full list of author information is available at the end of the article.

**Received:** 13 November 2018 | **Accepted:** 05 December 2018

start sites encoding for peroxisomal and mitochondrial isoforms (5). Over 150 disease-causing mutations have been identified in the *AGXT* gene (6). Approximately, 25% are insertions or deletions, while the other 75% are point mutations (3,7). The most common mutation found among PH1 patients is a G170R substitution, which causes mistargeting of the protein to mitochondria rather than peroxisomes (3). Other mutations are known to affect the protein's aggregation propensity, sensitivity to proteolytic degradation, catalytic efficiency, coenzyme binding affinity, and dimer stability (6). Surprisingly, despite the abundance known about disease-causing mutations and the structure and function of AGT, the genotype–phenotype relationship is difficult to predict for PH1. Patients with the same mutation, and even within the same family can vary in age of disease onset, disease severity, and responsiveness to pyridoxine (an AGT cofactor) therapy (3,4).

Animal models that accurately recapitulate the clinical phenotypes of human diseases are essential tools for the development of new therapies. This is particularly true for rare monogenic diseases, such as PH1, for which a better understanding of the genotype–phenotype relationship is needed for predicting clinical outcomes and developing treatment strategies. An *Agxt* null mouse was generated by Salido et al. (8), which displays hyperoxaluria like PH1 patients. Interestingly, not unlike the human condition, variations in disease severity have been reported by the different groups who have used this mouse model, particularly with regards to the development of nephrocalcinosis, despite the shared genetic background (8–10). The mouse model was created by targeted mutagenesis of the *Agxt* gene in embryonic stem cells (8). It was initially created on a mixed 129Sv/C57Bl/6 background (B6; 129Sv $Agxt^{tm1Ull}$ ) and then backcrossed with C57Bl/6 mice to create the B6.129Sv $Agxt^{tm1Ull}$  line (8). Both lines had elevated plasma and urine oxalate and glycolate levels. However, unlike patients, these mice did not spontaneously develop nephrocalcinosis. Renal CaOx stones were only observed after feeding 0.5%–0.7% ethylene glycol (EG), a precursor of glycolate and glyoxylate, in the drinking water (8), whereas Salido et al. (8) found that 4/6 *Agxt*<sup>-/-</sup> mice developed nephrocalcinosis after 3 weeks of 0.7% EG in drinking water, Castello et al. (10) found that only 6/21 *Agxt*<sup>-/-</sup> mice developed mild-to-moderate nephrocalcinosis following 4 weeks of 1.25% EG in drinking water. Thus, they concluded that the CaOx stone formation under 1.25% EG challenge is not a sensitive marker of disease in this mouse model. Based on variations in reported phenotypes of the previously developed *Agxt*<sup>-/-</sup> mouse, and recent advances in gene editing technology, we developed an *Agxt*<sup>-/-</sup> mouse model using CRISPR/Cas9 mediated gene editing. Development and characterization of this model are expected to provide valuable insights into possible causes of variability between groups, differences between mouse and human disease phenotypes, and potentially enable a better understanding of the genotype–phenotype

relationship. In addition, this mouse model will be useful for testing much needed novel therapies for PH1. Here, we describe the gene editing strategy, as well as the resulting phenotype of the constitutive *Agxt*<sup>-/-</sup> mouse.

## Subjects and Methods

### *Development of CRISPR/Cas9 Agxt<sup>-/-</sup> mice (C57Bl/6NTac-Agxt<sup>em4845Tac</sup>)*

All the animal studies were approved by the Institutional Animal Care and Use Committees at Taconic and Moderna. The targeting strategy was based on NCBI transcript NM\_016702.3. For technical reasons, CRISPR RNA (crRNA)/trans-activating crRNA (tracrRNA) hybrids instead of single guide RNA (sgRNA) molecules were co-injected into C57Bl/6NTac zygotes along with Cas9 protein. The goal of the targeting strategy was to delete exon 3, which should result in the loss of function of the *Agxt* gene by deleting part of the aminotransferase domain, and by generating a frameshift from exon 2 to exons 4–5 (premature stop codon in exon 4). Additionally, the resulting transcript may be a target for non-sense mediated RNA decay, and may therefore not be expressed at a significant level. Of all potential guide RNAs (gRNAs), the two used were chosen for their position and the lowest number of potential off-target sites. Six positive founder mice were identified, one of which showed the deletion of exon 3, with the junction of the gRNA cutting sites perfectly matching the predicted non-homologous end joining repair.

### *Genotyping*

Genomic DNA was extracted from single tail samples according to the Taconic Molecular Analysis Standard operating procedure and amplified using the provided primers: 13584\_5: AAAGCTCTGGGCTCAAAGC, 13584\_6: TCAGACGGAGGAAGACTTCC. The resulting polymerase chain reaction (PCR) product was gel isolated and purified. DNA samples were then sequenced in both directions using the above primers. The sequences were compared with the predicted CRISPR/Cas9-induced Nfam1 constitutive Knock-Out allele sequence. The PCR performed detects the CRISPR/Cas9-induced *Agxt* constitutive knock-out allele as well as potential insertion–deletion (indel) modifications and the unmodified *Agxt* wildtype (WT) allele. To distinguish indel modifications from unmodified WT sequences, a heteroduplex analysis (e.g., via capillary electrophoresis) was performed. Sizes of expected fragments (base pairs) were: 230 (del), 796(WT), and 796 (indel).

### *Ethylene glycol challenge*

Mice were given 0.7% or 1.2% EG in their drinking water (*ad libitum* for 3 weeks beginning at 10–12 weeks of age). Urine and plasma were collected at baseline and weekly thereafter. At the end of the study, liver, kidney, and bladder were collected for histological examination.

### ***Oxalate/glycolate/creatinine measurements***

Oxalate, glycolate, and creatinine concentrations were measured by Liquid chromatography-mass spectrometry (LC-MS)/MS. Sample analysis was performed on an Agilent 1200 series coupled with an AB Sciex API5500 using multiple reaction monitoring. Plasma glycolate and urine oxalate/glycolate samples were separated via reversed phase chromatography at room temperature on a 30 × 2.1 mm, 2.5 μm Waters HSS T3 column at 800 μl/minute in water with 0.1% formic acid and acetonitrile in 0.1% formic acid using positive electrospray ionization. Urine oxalate and glycolate elution gradients were 40%–60% over 45 seconds. Plasma glycolate gradients were 15%–35% over 20 seconds. For creatinine measurements, urine and plasma samples were separated via hydrophilic-interaction chromatography on a 50 × 2.1 mm, 1.7 μm Waters Acquity BEH Amide column at 600 μl/minute in 10 mM ammonium acetate 95:5 water:acetonitrile, and 10 mM ammonium acetate 95:5 acetonitrile:water using a 0%–10% elution gradient over 45 seconds using negative electrospray ionization.

### ***Quantitative reverse transcription PCR (RT-qPCR)***

Frozen liver tissues (~25–50 mg) were submerged in 1 ml (pre-chilled at –80°C) RNALater ICE (Thermo, catalog #AM7030) and stored at –20°C overnight. RNA was extracted using the Promega Maxwell RSC simplyRNA Tissue kit. Tissue was homogenized in 600 μl homogenization buffer using Zymo bashing beads and a Geno Grinder. Two hundred microliters homogenate was combined with 200 μl lysis buffer and loaded into a Maxwell purification instrument. Extracted RNA was eluted in 60 μl water and measured on the Agilent TapeStation for quality assessment and on the Thermo Qubit Fluoremeter for concentration. RNA was normalized to 10 ng/μl for quantitative PCR (qPCR) reaction. qPCR reactions were set up in triplicate and triplicates averaged for the analysis. Results compared to averaged expression in *Agxt<sup>+/+</sup>* mice. TaqMan assays used were from ThermoFisher Scientific: Mm00507980\_m1 (*Agxt1*), Mm01304088\_m1 (*Agxt2*), Mm00439249\_m (*Hao1*), and Mm99999915\_g1 (*Gapdh*—housekeeping gene).

### ***Immunoblot analysis***

Liver samples were homogenized using a Polytron PT 10-35 GT homogenizer or Precellys homogenizer. Protein was quantified in whole liver lysates or mitochondrial/peroxisomal fractions using the Pierce BCA assay kit. For immunoblotting, lysates (10 μg protein) were separated by sodium dodecyl sulfate-polyacrylamide gel electrophoresis SDS-PAGE. Membranes were incubated with anti-AGXT1 (NBPI-89200), anti-AGXT2 (PA5-57929), anti-HAO1 (ab172573), anti-catalase (LS-B2554), or anti-β-actin (CS-3700) antibodies. Membranes were imaged using the LiCOR imaging platform.

### ***Peroxisome isolation***

Peroxisomes were extracted from frozen liver tissue using the Peroxisome Isolation Kit (Sigma Aldrich PEROX1) according to the manufacturer's instructions. Briefly, liver samples (0.8–1.0 mg) were homogenized using a Polytron PT 10-35 GT homogenizer in 4 ml 1× peroxisome extraction buffer. The homogenate was centrifuged at 1,000 × *g* at 4°C for 10 minutes, the floating lipid layer was removed by aspiration, and the supernatant was transferred to a new tube. This step was repeated with 2,000 × *g* centrifugation. The supernatant was then centrifuged at 25,000 × *g* in an ultracentrifuge with a fixed angle rotor for 25 minutes at 4°C. The supernatant was discarded, and the pellet containing the crude peroxisomal fraction was resuspended in 600 μl 1× peroxisome extraction buffer. The crude peroxisomal fraction was then subject to density gradient centrifugation (100,000 × *g* at 4°C for 1.5 hours) to isolate the purified peroxisomal fraction (PPF). Following two PBS washes, the PPF was resuspended in 40 μl peroxisomal lysis buffer (1% Triton X-100, 1 mM Ethylenediaminetetraacetic acid (EDTA), 1-mM potassium phosphate, pH 7.7, supplemented with protease inhibitor) and subjected to three freeze-thaw cycles to lyse the peroxisomes. The lysed samples were then spun at 12,000 × *g* for 10 minutes and the supernatants were collected. Protein concentration was measured using the Pierce BCA Protein Assay Kit (ThermoFisher Scientific).

### ***AGT activity measurements***

AGT activity in purified peroxisomal fractions was assayed by measuring the pyruvate generated via the AGT catalyzed reaction of glyoxylate and L-alanine to produce glycine and pyruvate. Briefly, two sets of tubes were prepared with 10 μg of peroxisomal protein extract was mixed with 10 μl 1.25 mM pyridoxal 5'-phosphate, 25 μl 40 mM glyoxalate, and assay buffer (100 mM potassium phosphate, pH 7.7) to a final volume of 75 μl. To one set of tubes, 25 μl of 400 mM L-alanine was added to initiate the reaction. Both sets of tubes were incubated at 37°C for 3 hours shaking at 500 rpm. Tubes were then transferred to wet ice, and 25 μl of 50% aqueous trichloroacetic acid was added. L-alanine (25 μl) was then added to the “control” set of tubes to which it was not added previously. Samples were incubated on ice for 15 minutes, followed by centrifugation at 21,130 × *g* for 15 minutes at 4°C. Supernatants (15 μl) was then added in duplicate to a 96 well detection plate, followed by 60 μl Tris(hydroxymethyl)aminomethane (TRIS) (0.5 M, pH 8.0) and 25 μl coupling mix (2 μU/μl pyruvate oxidase, 50 μM FAD, 1 mM thiamine pyrophosphate (TPP), 0.23 μM Amplex UltraRed, 5 mM MgCl<sub>2</sub>, 5 mM EDTA, and horseradish peroxidase (HRP) in assay buffer). The plate was incubated at room temperature and then resorufin fluorescence was measured (excitation: 530 nm, emission: 590 nm). Fluorescence values from “control” samples were subtracted from samples given L-alanine as a substrate to control for endogenous pyruvate levels. Pyruvate generated was calculated based on a pyruvate standard curve.

### Histological analyses

Tissues were fixed in 10% neutral buffered formaldehyde solution, underwent routine paraffin processing and were embedded into paraffin blocks. Paraffin blocks were cut on a standard rotary microtome at 5 microns. Sections collected from each paraffin block were stained with hematoxylin and eosin (H&E) to assess morphology and a serial section was stained with Von Kossa for calcium staining. Briefly, after deparaffinization and hydration with distilled water, the glass slides were placed in 5% silver nitrate solution while exposed to an ultraviolet lamp. Glass slides were then rinsed in distilled water and placed in 5% sodium thiosulfate solution for 5 minutes. After rinsing in distilled water nuclear and cytoplasmic counterstaining was performed in a fast red solution for 5 minutes. Rinsing in distilled water, dehydration in alcohol, clearing in xylene, and mounting with Permount were final steps in Von Kossa's procedure for calcium staining. Glass slides were examined through a light microscope and color photographs were taken.

### Statistical analysis

Data are presented as the mean  $\pm$  standard error of the mean (SEM). Means were compared by unpaired (two groups), one-way, or two-way analysis of variance (ANOVA). Significant ANOVA findings were followed by Tukey's *post hoc* test for multiple comparisons. Two-tailed *p* values  $<0.05$  were considered as statistically significant. All the statistical analyses were performed using GraphPad Prism 7 software.

## Results

### CRISPR/Cas9 targeting strategy and confirmation of *Agxt* knockout

A mouse model with a constitutive knock-out of the *Agxt* gene was generated via CRISPR/Cas9-mediated gene editing. The gRNAs were chosen to cause deletion of exon 3, as this should result in loss of function of the *Agxt* gene by deleting a part of the aminotransferase domain and generating a frameshift from exon 2 to exons 4–5 (premature stop codon in exon 4) (Figure 1A). In addition, the resulting transcript could be a target for non-sense mediated RNA decay, and thus, not be expressed at a significant level. PCR analysis confirmed the desired genotype in founder mice (Figure 1B). To confirm the deletion of *Agxt* at the mRNA and protein levels, we performed qPCR and immunoblot analysis on liver lysates from *Agxt*<sup>-/-</sup> mice. The results confirmed that these mice have no *Agxt1* mRNA in the liver and no AGT protein in hepatic peroxisomal and mitochondrial fractions (Figure 1C and D). We also assayed AGT enzymatic activity in peroxisomal fractions from livers of *Agxt*<sup>-/-</sup> mice by measuring pyruvate generated via the AGT catalyzed the reaction of glyoxylate and L-alanine to produce glycine and pyruvate. We measured the activity of  $0.7 \pm 0.26$  and  $0.7 \pm 0.16$  pmol of pyruvate

produced/minute/ $\mu$ g of liver peroxisomes in male and female *Agxt*<sup>-/-</sup> mice, respectively, compared to 3.3 pmol/minute/ $\mu$ g in *Agxt*<sup>+/+</sup> littermates (Figure 1E).

### Urine and plasma glycolate and oxalate levels in *Agxt*<sup>-/-</sup> mice

To characterize the phenotype of the *Agxt*<sup>-/-</sup> mice, we performed a natural history study, in which we collected urine and plasma monthly up to 6 months of age, and then at 9 and 12 months of age. Thirty-one homozygous *Agxt*<sup>-/-</sup> mice (16F/15M) were enrolled in the study in addition to 20 *Agxt*<sup>+/+</sup> littermate controls. We measured urine oxalate and glycolate levels, as well as plasma glycolate levels, and found that as early as 5 weeks of age, levels of all three parameters were significantly elevated in male *Agxt*<sup>-/-</sup> mice, and urine oxalate and glycolate were elevated in female *Agxt*<sup>-/-</sup> mice compared to *Agxt*<sup>+/+</sup> controls (*p*  $< 0.05$ ) (Figure 2A). Surprisingly, urine oxalate levels returned to *Agxt*<sup>+/+</sup> levels by 8 weeks of age in females and were maintained there through 12 months of age. Consistent with previous reports in both rodents (11) and humans (12), males had higher plasma glycolate and urine oxalate levels than females, while urine glycolate levels were similar (Figure 2A). We also ran complete serum chemistry analyses and found no abnormalities in *Agxt*<sup>-/-</sup> mice at any time point (Table 1).

### Assessment of nephrocalcinosis in *Agxt*<sup>-/-</sup> mice

In addition to monitoring urine and plasma parameters, we also collected kidneys, bladder, and liver of mice at 12, 26, 39, and 52 weeks of age for histological examination. Von Kossa (VK) staining was done on kidney and bladder tissues to assess the development of nephrocalcinosis and/or urolithiasis. Focal, minimal deposition of brown, fine spiculated, and VK-positive crystalline material was occasionally noted within terminal medullary ducts of the papilla in *Agxt*<sup>-/-</sup> mice. These VK-positive depositions were observed in one female out of eight (four female/four male) at 12 weeks, one male out of eight (four female/four male) at 26 weeks, and one female and two males out of seven (four female/three male) at 52 weeks of age (Figure 2B). There was no evidence of the presence of VK-positive crystalline material in the examined kidney tissue slices collected from 39-week-old *Agxt*<sup>-/-</sup> mice or *Agxt*<sup>+/+</sup> mice of all age groups. Focal, minimal crystalline deposits were noted within the urothelium lining the pelvis of one, 26-week-old, male *Agxt*<sup>-/-</sup> mouse, and these were birefringent under polarized light (Figure 2C). All other animals were negative for urolithiasis.

### Effects of EG challenge on urine and plasma glycolate and oxalate and nephrocalcinosis

Since it was previously reported that EG feeding is necessary to induce nephrocalcinosis in the previously generated mouse models of PH1, we challenged the *Agxt*<sup>-/-</sup> mice with 0.7% or 1.2% EG in their drinking water for 3 weeks, beginning at 10–12 weeks of age. Urine and plasma were collected weekly for oxalate and glycolate measurements, and liver, kidney, and bladder were collected at the end of the third week for histological evaluation. As expected, EG

increased urine oxalate and glycolate, as well as plasma glycolate levels in both *Agxt<sup>+/+</sup>* and *Agxt<sup>-/-</sup>* mice. In male *Agxt<sup>-/-</sup>* mice, plasma glycolate levels were significantly elevated following 3 weeks of both 0.7% and 1.2% EG, whereas urine glycolate was only significantly increased at the 1.2% dose compared to *Agxt<sup>-/-</sup>* mice not given EG (Figure 3A). Urine oxalate levels were not significantly higher in male *Agxt<sup>-/-</sup>* mice given EG compared to those given regular water. In contrast, female mice were given 1.2% EG, but not 0.7% EG, had significantly elevated levels of all three parameters compared to *Agxt<sup>-/-</sup>* mice not given EG. Age-matched *Agxt<sup>+/+</sup>* controls given 1.2% EG had significantly elevated urine and plasma glycolate levels following 3 weeks of EG, but urine oxalate levels were not significantly different for either sex (Figure 3A). Consistent with data from the natural history study, urine oxalate and plasma glycolate levels were lower in female

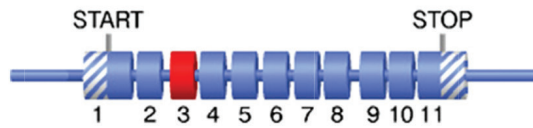
*versus* male *Agxt<sup>-/-</sup>* mice (both with and without EG). Urine glycolate levels, however, were similar between males and females. Histological assessment of kidneys showed focal, minimal deposition of VK-positive, fine crystalline material within the terminal collecting ducts of renal papillain 2/5 females and 0/5 males from the 0.7% EG group, and 2/5 females and 0/5 males from the 1.2% EG group (Figure 3B). Despite elevated oxalate and glycolate levels, there was no evidence of crystalline material in kidneys of *Agxt<sup>+/+</sup>* mice challenged with 1.2% EG. No histological abnormalities were observed in the liver or bladder from *Agxt<sup>-/-</sup>* or *Agxt<sup>+/+</sup>* mice.

***Agxt2 and Hao1 mRNA expression in Agxt<sup>-/-</sup> mice***

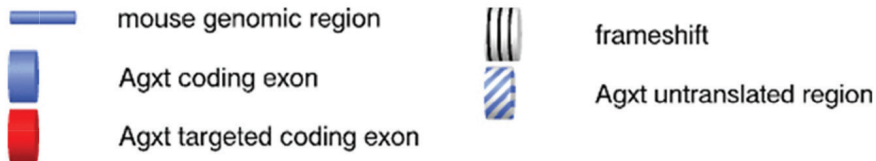
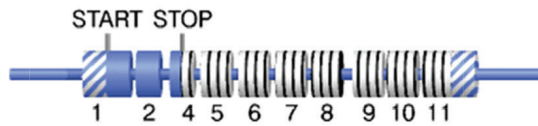
Since only a minority of our mice developed minimal nephrocalcinosis, even after 3 weeks of EG challenge,

**A**

**Mouse genomic locus**



**Targeted allele (after CRISPR/Cas9-mediated gene editing)**



**Proximal sgRNA**

```

TTGCATCTGT GGGAAAAGCA AGCCTCACAG AGCATGCTCC ACTTCACCTG TGGTAAAGCC ATGTGAGAGC CAGAATGAGT GCGGTCCCCC ACACTATTTC
AACGTAGACA CCCITTTTCGT TCGGAGTGTG TCGTACGAGG TGAAGTGGAC ACCATTTCGG TACACTCTCG GTCITACTCA CGCCAGGGGG TGTGATAAAG
                                     sgRNA1
TTGTGTATGT GTGTGTGTGT GTGTGTGTGT GTGTGTGTGT TAAATTTTTT TATTTGTAT TTTATTTCATT TACATTTCAA ATGTTGTITGC CCTTCCTGGT
AACACATACA CACACACACA CACACACACA CACACACACA ATTTAAAAAA ATAAACAATA AAATAAGTAA ATGTAAAGTT TACAACAACG GGAAGGACCA
TCCCCCTCCA CAACCCCCCA TTCCATCCCT CCTCCCCTTT GCCTCTATGA GGGTGTCTCG CCTCCCCTA CCCACTCCTG CCTTGCCAAT TACTCTGGG
AGGGGGAGGT GTTGGGGGGT AAGGTAGGGA GGAGGGGAAA CGGAGATACT CCCACGAGG GGAGGGTGTG GGTGAGGAC GGAACGGTTA ATGTGACCCC
CATCAAGCCT ACACAGGACC AAGGGCCTCT CCTCCATTG ATGCCAGATA AGGCCATCTT CGGCTACATA TATGGCTGGA GCCATGGGTC CTCCTGTGT
GTAGTTCGGA TGTGTCTCG TTCCCGGAGA GGAGGGTAAC TACGGTCTAT TCCGGTAGAA GCCGATGTAT ATACCCGACCT CGGTACCCAG GAGGGACACA
ACTCTTTAGT TGGTGGTTTA GTCCTGGGA GCTCTGGTTG ATTCGGTTAG TTGATATTGT TCTTCTATG GGGTTCAGT CCCCTTCAGC TCCTTCGGTC
TGAGAAATCA ACCACCAAT CAGGGACCT CGAGACCAAC TAAGCCAATC AACTATAACA AGAAGGATAC CCCAACGTC GGGGAAGTCG AGGAAGCCAG
                                     exon_3
CTTCCCCTCC CCCCACTAT GTCTAACTCA CCACCCATTC TGTCCTGTG ATCAGGAGCC CGTGTGCACC AGATGATCAA GAAGCCTGGA GAACATTATA
GAAGGGGAGG GGGTGTGATA CAGATTGAGT GGTGGTAAG ACAGGGACAG TAGTCTCCGG GCACACGTGG TCTACTAGTT CTTCGGACCT CTTGTAATAT
    
```

**Distal sgRNA**

```

                                     exon_3
CACTGCAGGA GGTGGAGGAG GTACTGAGAC ACCGGAATCA TCGTTGGTGG GGTGGCTGG AATTCTGAGG CCTATGGCTT GACTTCTCAG TGCTAAGAC
GTGACGTCTC CCACCTCTCC CATGACTCTG TGGCCTTAGT AGCAACCACC CCAACCGACC TTAAGACTCC GGATACCGAA CTGAAGAGTC ACAGATTCTG
    
```

*continued*

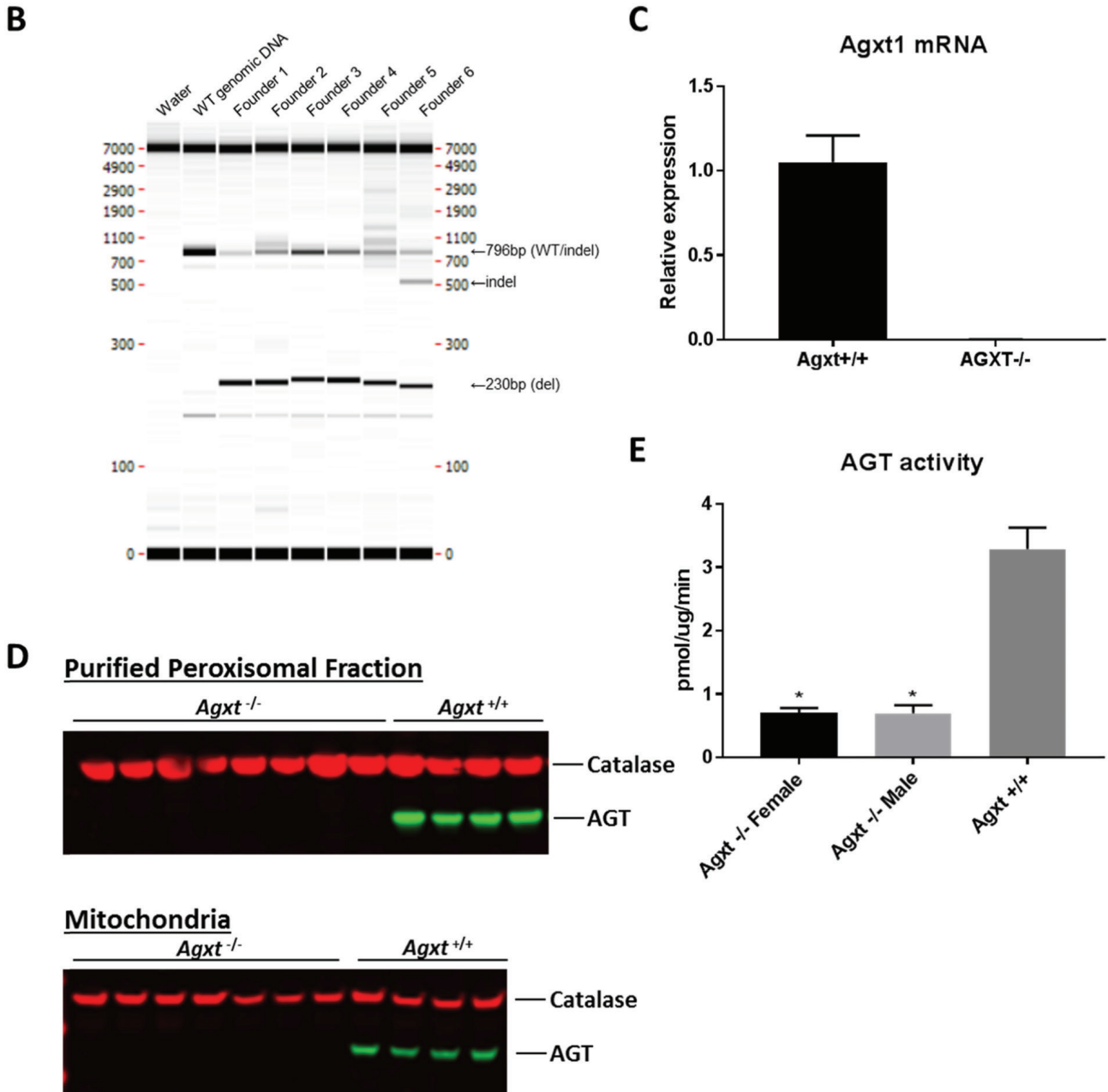


**Figure 1.** *Agxt* targeting strategy and confirmation of *Agxt* knockout. (A) Targeting strategy for CRISPR/Cas9 mediated editing of the *Agxt* gene. (B) PCR analysis of potential founder mice. (C) RT-PCR analysis of liver samples to confirm the absence of *Agxt1* mRNA in *Agxt*<sup>-/-</sup> mice. (D) Western blot analysis of liver peroxisomal and mitochondrial fractions to confirm the absence of AGT protein in *Agxt*<sup>-/-</sup> mice. (E) AGT activity in the liver peroxisomal fraction of *Agxt*<sup>+/+</sup> and *Agxt*<sup>-/-</sup> mice. N = 4/group. \*p < 0.05, one-way ANOVA followed by Dunnett's multiple comparisons test.

we investigated the expression levels of other enzymes involved in glyoxylate metabolism to see if these could be preventing the buildup of oxalate. We measured mRNA levels of *Agxt2*, which encodes for the protein AGT2 (a mitochondrial analog of AGT, which can also metabolize glyoxylate), and hydroxy acid oxidase 1 (*Hao1*), which encodes for the protein glycolate oxidase (GO). GO converts excess glycolate in peroxisomes to glyoxylate, thus increasing substrate for AGT. We performed qPCR

and immunoblot analysis on liver samples from *Agxt*<sup>-/-</sup> mice and *Agxt*<sup>+/+</sup> littermates and found no differences in *Agxt2* mRNA or protein levels (Figure 4A and B). *Hao1* mRNA levels were also unchanged between *Agxt*<sup>-/-</sup> and *Agxt*<sup>+/+</sup> mice, but consistent with previously published reports that *Hao1* is hormonally regulated, we found lower expression of both *Hao1* mRNA and GO protein in females versus males of both genotypes (data not shown). Surprisingly, GO protein levels were higher in *Agxt*<sup>-/-</sup>

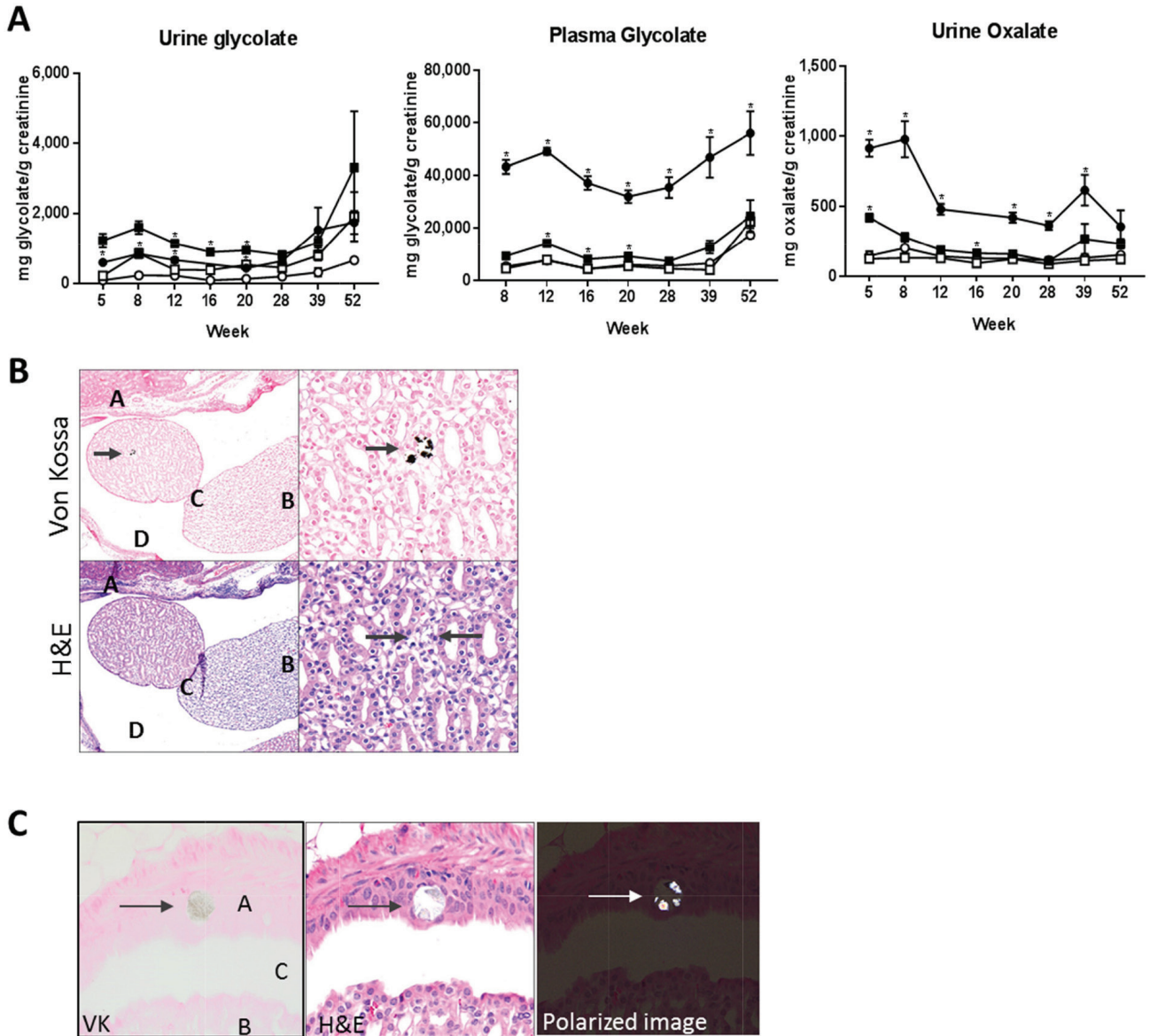


**Figure 2.** Natural history study of *Agxt*<sup>-/-</sup> mice. (A) Measurements of urine glycolate, plasma glycolate, and urine oxalate in male and female *Agxt*<sup>-/-</sup> mice from 5 weeks of age to 1 year. Black circles: male *Agxt*<sup>-/-</sup>, black squares: female *Agxt*<sup>-/-</sup>, open circles: male *Agxt*<sup>+/+</sup>, open squares: female *Agxt*<sup>+/+</sup> (B) VK-positive crystalline material in terminal medullary ducts of renal papilla (arrows) in a 52-week-old male *Agxt*<sup>-/-</sup> mouse. (C) Birefringent (under polarized light) VK-positive crystalline material in urothelium lining the pelvis (arrows) of a 26-week-old male *Agxt*<sup>-/-</sup> mouse. H&E: Hematoxylin & Eosin; VK: VonKossa; A: Cortex; B: Inner Medulla; C: Collecting ducts of the medulla; D: Pelvis. N = 3–16. \*p < 0.05 by multiple t-tests with Holm-Sidak method for multiple comparisons.

versus *Agxt*<sup>+/+</sup> mice (Figure 4B). To our knowledge, this finding has not been reported in the previously generated mouse models of PH1.

## Discussion

We have generated and characterized an *Agxt*<sup>-/-</sup> mouse model on a C57Bl/6 background via CRISPR/Cas9 gene editing (Figure 1A–E). We found elevated levels of urine glycolate and oxalate and plasma oxalate compared to *Agxt*<sup>+/+</sup> mice (Figure 2A), like the levels reported in previously generated *Agxt* null mice (8). Despite

these elevated biomarkers, only a small subset of mice developed minimal spontaneous nephrocalcinosis (Figure 2B) and only one mouse developed urolithiasis (Figure 2C) over the course of 1 year. Even when challenged with 0.7% or 1.2% EG in their drinking water, which further increased urine and plasma glycolate and oxalate levels (Figure 3A), only a minority of *Agxt*<sup>-/-</sup> animals developed minimal nephrocalcinosis as demonstrated by the presence of fine crystalline material in the terminal collecting ducts of the renal papilla (Figure 3B). *Agxt2* mRNA and corresponding AGT2 protein were still expressed in the *Agxt*<sup>-/-</sup> animals at similar levels as in

**Table 1.** Blood chemistry parameters in *Agxt<sup>+/+</sup>* and *Agxt<sup>-/-</sup>* mice. Data presented as mean  $\pm$  standard deviation. N = 4–8/group. ND: No data.

	12 wk		26wk		39wk		52wk	
	<i>Agxt<sup>+/+</sup></i>	<i>Agxt<sup>-/-</sup></i>	<i>Agxt<sup>+/+</sup></i>	<i>Agxt<sup>-/-</sup></i>	<i>Agxt<sup>+/+</sup></i>	<i>Agxt<sup>-/-</sup></i>	<i>Agxt<sup>+/+</sup></i>	<i>Agxt<sup>-/-</sup></i>
ALP (U/L)	ND	ND	64.2 $\pm$ 15.8	68.4 $\pm$ 22.6	79.4 $\pm$ 35.6	74.9 $\pm$ 32.7	77.2 $\pm$ 33.1	88.3 $\pm$ 35.9
AST (U/L)	ND	ND	137.2 $\pm$ 144	176.1 $\pm$ 131.9	67.4 $\pm$ 12.6	69 $\pm$ 22.5	253.6 $\pm$ 390.6	312.9 $\pm$ 253.9
ALT (U/L)	41.6 $\pm$ 15.6	81 $\pm$ 99.4	37.8 $\pm$ 9.8	53.9 $\pm$ 22.4	45.4 $\pm$ 9.2	42.9 $\pm$ 9.5	176.6 $\pm$ 270.4	200 $\pm$ 194.9
Creatine Kinase (U/L)	ND	ND	1134.6 $\pm$ 1720.6	3511.3 $\pm$ 4911.6	95.4 $\pm$ 64.8	123.3 $\pm$ 63.2	417 $\pm$ 87.2	858.3 $\pm$ 439.1
Albumin (g/dL)	3.28 $\pm$ 0.3	3.3125 $\pm$ 0.2	3.2 $\pm$ 0.2	3.2 $\pm$ 0.2	3.2 $\pm$ 0.2	3.3 $\pm$ 0.1	2.9 $\pm$ 0.2	2.9 $\pm$ 0.1
Total bilirubin (mg/dL)	ND	ND	0.2 $\pm$ 0	0.2 $\pm$ 0	0.2 $\pm$ 0.1	0.1 $\pm$ 0	0.2 $\pm$ 0.1	0.2 $\pm$ 0.1
Total Protein (g/dL)	ND	ND	5.5 $\pm$ 0.2	5.4 $\pm$ 0.1	5.6 $\pm$ 0.3	5.7 $\pm$ 0.2	4.8 $\pm$ 0.9	5.2 $\pm$ 0.1
Globulin (g/dL)	ND	ND	2.3 $\pm$ 0.1	2.2 $\pm$ 0.1	2.4 $\pm$ 0.1	2.4 $\pm$ 0.1	1.9 $\pm$ 0.9	2.2 $\pm$ 0.1
Bilirubin - Conjugated (mg/dL)	ND	ND	0 $\pm$ 0	0.1 $\pm$ 0.1				
BUN (mg/dL)	16.8 $\pm$ 1.1	18.75 $\pm$ 2.5	16.4 $\pm$ 2.4	17.3 $\pm$ 2.8	14.4 $\pm$ 2.4	14 $\pm$ 1.7	21.6 $\pm$ 12.5	23.7 $\pm$ 3.5
Creatinine (mg/dL)	ND	ND	0.2 $\pm$ 0.1	0.2 $\pm$ 0.1	0.2 $\pm$ 0	0.2 $\pm$ 0	0.2 $\pm$ 0.1	0.2 $\pm$ 0.1
Cholesterol (mg/dL)	113.6 $\pm$ 15	123 $\pm$ 15.9	116.2 $\pm$ 11	111.9 $\pm$ 19.5	105.6 $\pm$ 21.4	101.8 $\pm$ 20.6	97.8 $\pm$ 22.1	93.1 $\pm$ 20.2
Glucose (mg/dL)	206.6 $\pm$ 78.5	223 $\pm$ 39.1	203.4 $\pm$ 33.7	160 $\pm$ 27	198.4 $\pm$ 26.4	183.4 $\pm$ 21.9	256.8 $\pm$ 23	247.6 $\pm$ 20.4
Calcium (mg/dL)	ND	ND	9.5 $\pm$ 0.3	9.3 $\pm$ 0.1	10.3 $\pm$ 0.1	10.4 $\pm$ 0.3	10.5 $\pm$ 0.5	10.2 $\pm$ 0.2
Phosphorus (mg/dL)	ND	ND	8.6 $\pm$ 1.2	9.3 $\pm$ 1.2	9.8 $\pm$ 0.6	11.4 $\pm$ 1.2	11.5 $\pm$ 1.5	11.9 $\pm$ 1.2
Bicarbonate TCO2 (mmol/L)	ND	ND	28.2 $\pm$ 1.1	26.3 $\pm$ 2.5	27.4 $\pm$ 1.5	25.9 $\pm$ 2.9	24.2 $\pm$ 4.3	26 $\pm$ 3.6
Chloride (mmol/L)	ND	ND	106.8 $\pm$ 2.3	108 $\pm$ 1.5	105.2 $\pm$ 2.9	106 $\pm$ 1.6	106.8 $\pm$ 3	106.9 $\pm$ 3.4
Potassium (mmol/L)	ND	ND	7.4 $\pm$ 0.6	6.8 $\pm$ 0.4	7.5 $\pm$ 0.9	7.8 $\pm$ 0.6	9.1 $\pm$ 1	8.8 $\pm$ 0.7
ALB/GLOB ratio	ND	ND	1.4 $\pm$ 0.1	1.5 $\pm$ 0.1	1.3 $\pm$ 0.1	1.4 $\pm$ 0.1	2.9 $\pm$ 3.8	1.3 $\pm$ 0
Sodium (mmol/L)	ND	ND	148.2 $\pm$ 0.8	149.5 $\pm$ 3.3	151.4 $\pm$ 4	151.8 $\pm$ 2.6	149.3 $\pm$ 3.3	149.1 $\pm$ 3.7
BUN/Creatinine Ratio	ND	ND	115 $\pm$ 48.1	95.6 $\pm$ 32.5	89 $\pm$ 46.3	70 $\pm$ 8.5	71 $\pm$ 70	167.1 $\pm$ 59.9
Bilirubin - Unconjugated (mg/dL)	ND	ND	0.2 $\pm$ 0	0.2 $\pm$ 0	0.2 $\pm$ 0.1	0.1 $\pm$ 0	0.2 $\pm$ 0.1	0.2 $\pm$ 0.1
NA/K Ratio	ND	ND	20.2 $\pm$ 1.8	22. $\pm$ 1.6	20.4 $\pm$ 2.6	19.5 $\pm$ 1.6	16.5 $\pm$ 2.1	17 $\pm$ 1.6

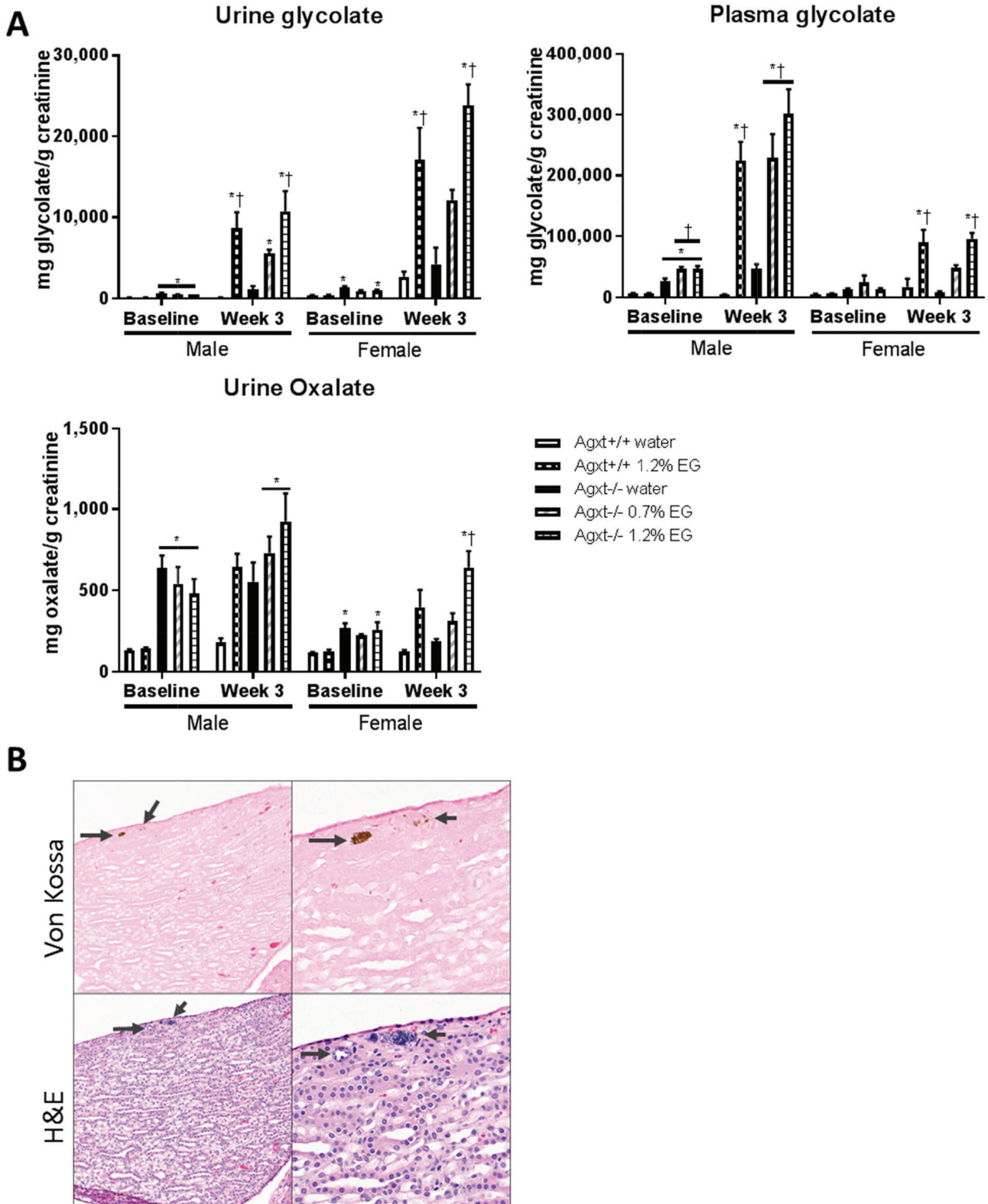


**Figure 3.** Effects of EG challenge on *Agxt*<sup>-/-</sup> mice. (A) Measurements of urine glycolate, plasma glycolate, and urine oxalate in male and female *Agxt*<sup>+/+</sup> and *Agxt*<sup>-/-</sup> mice at baseline and following 3 weeks of 0.7% or 1.2% EG in their drinking water. (B) VK-positive crystalline material in terminal medullary ducts of the renal papilla (arrows) of a female *Agxt*<sup>-/-</sup> mouse following 3 weeks of 0.7% EG. H&E: Hematoxylin & Eosin; VK: Von Kossa. N = 4–6/group. \**p* < 0.05 versus *Agxt*<sup>+/+</sup> water, †*p* < 0.05 versus *Agxt*<sup>-/-</sup> water, one-way ANOVA followed by Tukey multiple comparisons test.

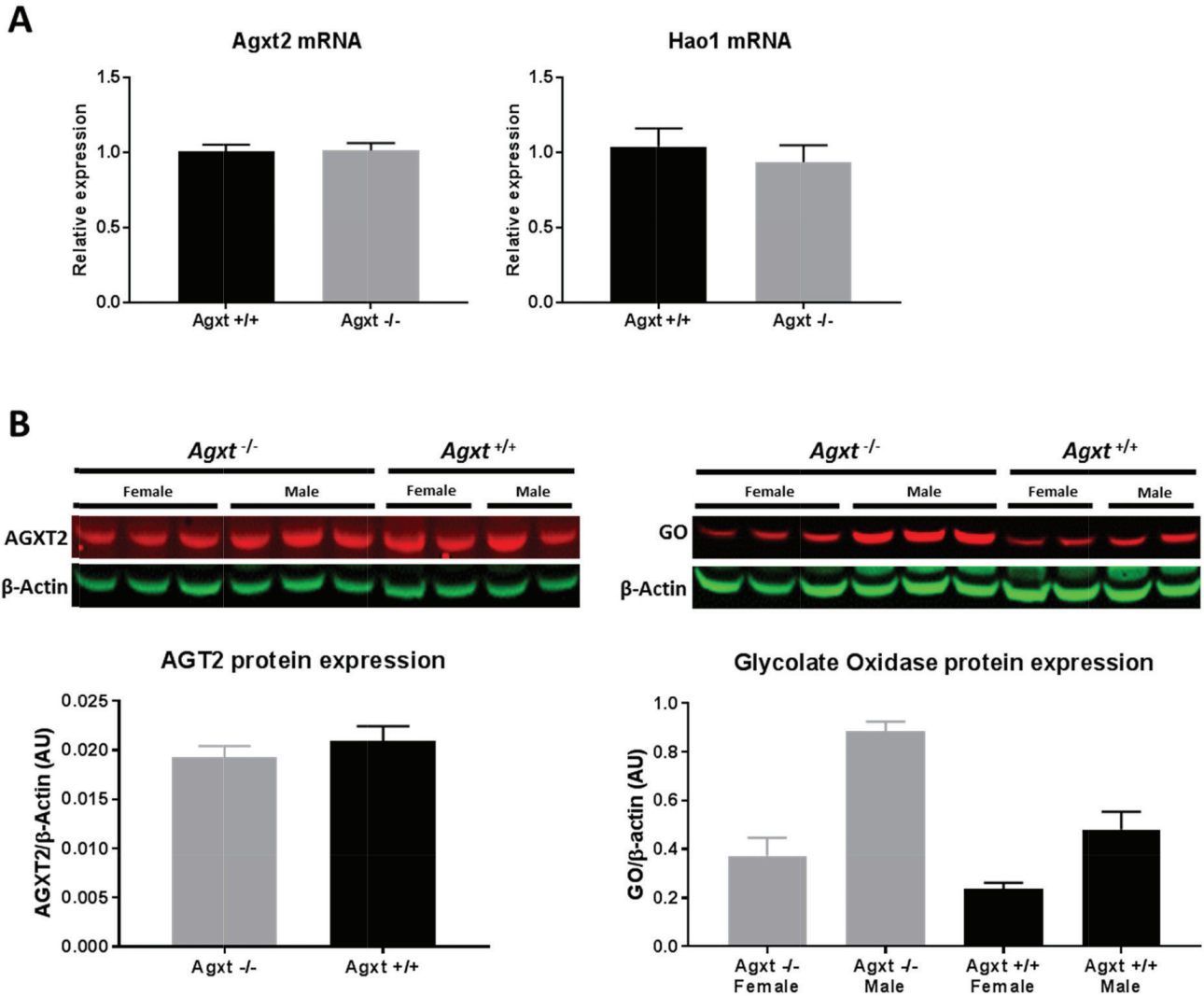


**Figure 4.** *Agxt2* and *Hao1* expression in livers of *Agxt*<sup>-/-</sup> mice analysis of (A) mRNA and (B) protein levels of *Agxt2* (protein name: AGT2) and *Hao1* (protein name: Glycolate Oxidase) in the liver of *Agxt*<sup>+/+</sup> and *Agxt*<sup>-/-</sup> mice. N = 2–6/group.

*Agxt*<sup>+/+</sup> mice (Figure 4A and B). Surprisingly, although *Hao1* mRNA expression in liver was similar between *Agxt*<sup>-/-</sup> and *Agxt*<sup>+/+</sup> mice (Figure 4A), corresponding GO protein expression was higher in *Agxt*<sup>-/-</sup> mice (Figure 4B). This suggests that rates of *Hao1* translation or GO degradation may be altered in *Agxt*<sup>-/-</sup> mice, which requires further study and should be considered when developing therapies for PH1. Well-characterized animal models of human diseases are critical for testing novel therapies, particularly for rare diseases like PH1. It can be challenging when species differences prevent an animal model from accurately recapitulating the clinical phenotype of patients. Like the previously generated *Agxt*<sup>-/-</sup> mouse model, our CRISPR/Cas9 *Agxt*<sup>-/-</sup> mice had elevated urine and plasma glycolate and oxalate levels like PH1 patients. However, unlike patients, our *Agxt*<sup>-/-</sup> mice developed only minimal nephrocalcinosis. Similarly, an induced rat model of PH1 was created using *Agxt* siRNA in addition to 1% EG in the drinking water (13), and

like the mice, these rats displayed hyperoxaluria but did not develop nephrocalcinosis. It is well established that rodents do not develop nephrocalcinosis at the rate or to the degree that humans do unless challenged with EG or other precursors of glyoxylate (14,15). One reason is their higher glomerular filtration rate, which allows them to clear excess oxalate more effectively (9). Even when challenged with 0.7% or 1.2% EG in their drinking water, we found that only a minority of *Agxt*<sup>-/-</sup> mice developed nephrocalcinosis. This is in line with reports by Castello et al. (10), whereas Salido et al. (8) found that 0.7% EG in drinking water was sufficient to cause nephrocalcinosis in 4/6 mice. Harsher methods than EG in drinking water can be used to induce nephrolithiasis in mice, such as oxalate, glyoxylate or hydroxyproline in the diet (14,15), or intra-abdominal glyoxylate injection (16). Additionally, it has been reported that calcium supplementation may be necessary to induce the formation and deposition of CaOx crystals mice (4,11,12,17–19).

For monogenic diseases like PH1, replacement of the missing gene or protein is the most straightforward therapeutic strategy. Since AGT is an intracellular protein localized to the peroxisome, enzyme replacement therapy is not possible due to drug delivery hurdles. Gene therapy using adeno-associated viral (AAV) vectors has been tested in *Agxt* null mice and resulted in a reduction of hyperoxaluria and prevention of oxalate crystals in the urine (8–10). However, AAV mediated gene therapy does come with safety concerns, including neutralizing antibodies, and genotoxicity. An alternative to gene therapy that would also replace the missing enzyme inside of cells is messenger RNA (mRNA) therapy. This therapeutic modality would instruct the body to produce its own AGT enzyme in hepatocytes but does not incorporate permanently into the genome, thus alleviating some of the safety concerns of traditional gene therapy. mRNA therapy has recently shown efficacy in preclinical models of other inborn errors of metabolism, such as methylmalonic acidemia (20) and acute intermittent porphyria (21). Another treatment strategy for PH1 is the manipulation of other aspects of the glyoxylate metabolism pathway. Small interfering RNA (siRNA) mediated knockdown of GO (13,22,23) or hepatic lactate dehydrogenase (24) have been tested in mouse and rat models of PH1 with the aim of decreasing oxalate production by hepatocytes. These strategies seem promising, but there is always a concern of unintended effects when disrupting more genes than those already impacted by the disease.

## Conclusion

In summary, we have created a mouse model which resembles much of the clinical phenotype of PH1 patients using CRISPR/Cas9 mediated gene editing. Although this mouse does not develop spontaneous nephrocalcinosis and urolithiasis to the degree that patients do, it will still be a useful tool in the development of much needed new therapies for this devastating disease.

## Acknowledgments

The authors would like to thank Taconic for creating the *Agxt*<sup>-/-</sup> mouse, Charles River Laboratories (formerly Agilux) for performing the oxalate and glycolate measurements, and the University of Massachusetts Medical School for histological tissue processing and staining.

## Funding

All studies were funded by Moderna, Inc (Cambridge, MA).

## Declaration of conflicting interests:

All authors are current or previous employees of and received salary and stock options from Moderna, Inc (Cambridge, MA).

## Ethical Approval

All applicable international, national, and/or institutional guidelines for the care and use of animals were followed.

## Consent for publication

Not applicable.

## Author details

Kimberly A. Coughlan<sup>1</sup>, Rajanikanth J. Maganti<sup>1</sup>, Andrea Frassetto<sup>1</sup>, Christine M. DeAntonis<sup>1</sup>, Meredith Wolfrom<sup>1</sup>, Anne-Renee Graham<sup>1</sup>, Shawn M. Hillier<sup>1</sup>, Steven Fortucci<sup>1</sup>, Hoor Al Jandal<sup>1</sup>, Sue-Jean Hong<sup>1</sup>, Paloma H. Giangrande<sup>1</sup>, Paolo G. V. Martini<sup>1</sup>

1. Rare Diseases, Moderna Inc, Cambridge, MA

## References

- Martin-Higueras C, Torres A, Salido E. Molecular therapy of primary hyperoxaluria. *J Inherit Metab Dis* 2017; 40(4):481–9. <https://doi.org/10.1007/s10545-017-0045-3>
- Cochat P, Deloraine A, Rotily M, Olive F, Liponski I, Deres N. Epidemiology of primary hyperoxaluria type 1. *Nephrol Dial Transpl* 1995; 10(suppl8):3–7. <https://doi.org/10.1093/ndt/10.suppl8.3>
- Williams EL, Acquaviva C, Amoroso A, Chevalier F, Coulter-Mackie M, Monico CG, et al. Primary hyperoxaluria type 1: update and additional mutation analysis of the AGXT gene. *Human Mutat* 2009; 30(6):910–7. <https://doi.org/10.1002/humu.21021>
- Cellini B, Oppici E, Paiardini A, Montioli R. Molecular insights into primary hyperoxaluria type I pathogenesis. *Front Biosci* 2012; 17(1):621. <https://doi.org/10.2741/3948>
- Holbrook JD, Birdsey GM, Yang Z, Bruford MW, Danpure CJ. Molecular adaptation of alanine: glyoxylate aminotransferase targeting in primates. *Mol Biol Evol* 2000; 17(3):387–400. <https://doi.org/10.1093/oxfordjournals.molbev.a026318>
- Oppici E, Montioli R, Cellini B. Liver peroxisomal alanine: glyoxylate aminotransferase and the effects of mutations associated with Primary Hyperoxaluria Type I: an overview. *Biochimica Et Biophysica Acta Bba Proteins Proteom* 2015; 1854(9):1212–9. <https://doi.org/10.1016/j.bbapap.2014.12.029>
- Tarn A, von Schnakenburg C, Rumsby G. Primary hyperoxaluria type 1: diagnostic relevance of mutations and polymorphisms in the alanine: glyoxylate aminotransferase gene (AGXT). *J Inherit Metab Dis* 1997; 20(5):689–96. <https://doi.org/10.1023/A:1005326510239>
- Salido EC, Li XM, Lu Y, Wang X, Santana A, Roy-Chowdhury N, et al. Alanine-glyoxylate aminotransferase-deficient mice, a model for primary hyperoxaluria that responds to adenoviral gene transfer. *Proc Natl Acad Sci* 2006; 103(48):18249–54. <https://doi.org/10.1073/pnas.0607218103>
- Salido E, Rodriguez-Pena M, Santana A, Beattie SG, Petry H, Torres A. Phenotypic correction of a mouse model for primary hyperoxaluria with adeno-associated virus gene transfer. *Mol Ther* 2011; 19(5):870–5. <https://doi.org/10.1038/mt.2010.270>
- Castello R, Borzone R, D'Aria S, Annunziata P, Piccolo P, Brunetti-Pierri N. Helper-dependent adenoviral vectors for liver-directed gene therapy of primary hyperoxaluria type 1. *Gene Ther* 2015; 23(2):129–34. <https://doi.org/10.1038/gt.2015.107>
- Richardson K. Effect of testosterone on the glycolic acid oxidase levels in male and female

- rat liver. *Endocrinology* 1964; 74(1):128–32. <https://doi.org/10.1210/endo-74-1-128>
12. Hesse A, Klocke K, Classen A, Vahlensieck W. Age and sex as factors in oxalic acid excretion in healthy persons and calcium oxalate stone patients. *Contrib Nephrol* 1987; 58:16–20. <https://doi.org/10.1159/000414479>
  13. Liebow A, Li X, Racie T, Hettinger J, Bettencourt BR, Najafian N, et al. An investigational RNAi therapeutic targeting glycolate oxidase reduces oxalate production in models of primary hyperoxaluria. *J Am Soc Nephrol* 2016; 28(2):ASN.2016030338. <https://doi.org/10.1681/ASN.2016030338>
  14. Khan S, Glenton P, Byer K. Modeling of hyperoxaluric calcium oxalate nephrolithiasis: experimental induction of hyperoxaluria by hydroxy-L-proline. *Kidney Int* 2006; 70(5):914–23. <https://doi.org/10.1038/sj.ki.5001699>
  15. Khan S. Animal models of kidney stone formation: an analysis. *World J Urol* 1997; 15(4):236–43. <https://doi.org/10.1007/BF01367661>
  16. Okada A, Nomura S, Higashibata Y, Hirose M, Gao B, Yoshimura M, et al. Successful formation of calcium oxalate crystal deposition in mouse kidney by intraabdominal glyoxylate injection. *Urol Res* 2007; 35(2):89–99. <https://doi.org/10.1007/s00240-007-0082-8>
  17. Khan SR, Glenton PA. Experimental induction of calcium oxalate nephrolithiasis in mice. *J Urol* 2010; 184(3):1189–96. <https://doi.org/10.1016/j.juro.2010.04.065>
  18. Fischer AW, Cannon B, Nedergaard J. Optimal housing temperatures for mice to mimic the thermal environment of humans: an experimental study. *Mol Metab* 2018; 7:161–70. <https://doi.org/10.1016/j.molmet.2017.10.009>
  19. Martin-Higueras C, Luis-Lima S, Salido E. Glycolate oxidase is a safe and efficient target for substrate reduction therapy in a mouse model of primary hyperoxaluria type I. *Mol Ther* 2016; 24(4):719–25. <https://doi.org/10.1038/mt.2015.224>
  20. An D, Schneller JL, Frassetto A, Liang S, Zhu X, Park J-S, et al. Systemic messenger RNA therapy as a treatment for methylmalonic acidemia. *Cell Rep* 2017; 21(12):3548–58. <https://doi.org/10.1016/j.celrep.2017.11.081>
  21. Jiang L, Berraondo P, Jericó D, Guey LT, Sampedro A, Frassetto A, et al. Systemic messenger RNA as an etiological treatment for acute intermittent porphyria. *Nat Med* 2018; 24(12):1899–1909. <https://doi.org/10.1038/s41591-018-0199-z>
  22. Dutta C, Avitahl-Curtis N, Pursell N, Cohen M, Holmes B, Diwanji R, et al. Inhibition of glycolate oxidase with dicer-substrate siRNA reduces calcium oxalate deposition in a mouse model of primary hyperoxaluria type 1. *Mol Ther* 2016; 24(4):770–8. <https://doi.org/10.1038/mt.2016.4>
  23. Milliner DS. siRNA therapeutics for primary hyperoxaluria: a beginning. *Mol Ther* 2016; 24(4):666–7. <https://doi.org/10.1038/mt.2016.50>
  24. Lai C, Pursell N, Gierut J, Saxena U, Zhou W, Dills M, et al. Specific inhibition of hepatic lactate dehydrogenase reduces oxalate production in mouse models of primary hyperoxaluria. *Mol Ther* 2018; 26(8):1983–95. <https://doi.org/10.1016/j.ymthe.2018.05.016>